ISSN 0915-633X

NATIONAL INSTITUTE FOR FUSION SCIENCE

Losses of Neutral Beam Injected Fast Ions Due to Adiabaticity Breaking Processes in a Field-Reversed Configuration

T. Takahashi, K. Inoue, N. Iwasawa, T. Ishizuka and Y. Kondoh

(Received - Jan. 6, 2004)

NIFS-791 Feb. 2004

RESEARCH REPORT
NIFS Series

TOKI, JAPAN

Losses of neutral beam injected fast ions due to adiabaticity breaking processes in a Field-Reversed Configuration

Toshiki Takahashi, Koji Inoue, Naotaka Iwasawa *, Takashi Ishizuka, and Yoshiomi Kondoh

Department of Electronic Engineering, Gunma University, Kiryu, Gunma 376-8515, Japan

** Satellite Venture Business Laboratory, Gunma University, Kiryu, Gunma 376-8515, Japan*

Losses of neutral beam (NB) injected fast ions from the confinement region of a Field-Reversed Configuration (FRC) with a strong magnetic mirror are numerically analyzed for parameters relevant to NB injection experiments on the FIX (FRC injection experiment) device [T. Asai *et al.*, Phys. Plasmas 7, 2294 (2000)]. Ionization processes of beam particles are calculated by the Monte Carlo method. The confinement of beam ions is discussed with the concept of accessible regions that restrict the ion excursion and are determined from two constants of motion, the kinetic energy and canonical angular momentum, in the case of an axisymmetric and a steady state FRC without an electrostatic field. From the calculation of the accessible regions, it is found that all the fast ions suffer from the orbit loss on the wall surface and/or the end loss. Single particle orbits are also calculated to find a difference of confinement properties from the results by employing the accessible regions. The magnetic moment is observed to show non-adiabatic motions of the beam ions, which cause a gradual orbit loss on the wall even in a case that a strong magnetic mirror is applied. The results show that the correlation of the magnetic moment disappears as the fast ions experience the density gradient around the separatrix surface and the field-null points.

I. INTRODUCTION

Field-Reversed Configurations[1] (FRCs) have no appreciable toroidal field and are self-sustained by the toroidal plasma current. Consequently, their plasma beta is extremely high. The averaged beta value $\langle\beta\rangle$ is in the range 0.82-0.92, which is estimated from the relation[2] $\langle\beta\rangle \approx 1 - x_s^2/2$ and the experimental results of x_s (the ratio of the separatrix radius r_s to the wall radius r_w) being in the range 0.4-0.6.[1] The synchrotron radiation loss that is a dominant energy loss mechanism in a high temperature fusion plasma is mitigated in this high beta FRC plasma. The conceptual design study of a D-^{3}He fueled FRC fusion reactor, ARTEMIS[3,4], is based on an elegant utilization of surplus power. The toroidal plasma current of the FRCs, which sustains a poloidal magnetic field for plasma confinement, however, soon decays due to an anomalous resistivity[1]. Therefore, improvement of particle, momentum and energy confinements is a key issue for the fusion application. Also, technologies of external inputs of particle, momentum, and energy should be developed to sustain the FRC plasma at a steady state.

The experiment of neutral beam (NB) injection into an FRC was started at the FIX (FRC injection experiment) device[5] in order to improve the confinements, and some new results are obtained.[6-10] The NB injection prolongs up to 240 % the e-folding FRC lifetime,[6, 7] and a stabilization mechanism induced by NB injection probably reduces the level of global motion[10]; it is a possibility of improvement of confinements. Electron heating is also observed by the Thomson scattering diagnostics.[11] It is interesting to study a deposition power density to electrons and its influence on global behavior.

In order to understand the effect of the NB injection on global characteristics of FRC, a detailed analysis on beam ion motion is necessary. High-energetic beam ions often travel the open mirror region, i.e., outside the separatrix. Thus the beam ion confinement depends on the strength of magnetic mirror. Therefore, a study of beam ion motion in various equilibria of FRC, in particular a computation on beam ion trap in different magnetic mirror, is of great importance. In Refs. 6 and 7, the trapped fraction of beam ions was numerically calculated. Asai's work showed its

dependency on the mirror ratio R_M ; it is increasing up to 100 % as $R_M \to 9$. A definite description of the trapped duration time of beam ions in an FRC, however, is not shown in both Refs. 6 and 7. The collisionless pitch angle scattering in the vicinity of X-point causes a non-adiabatic ion motion, and resultantly the ion orbit becomes ergodic as it passes through the neighborhood of X-point.[12, 13] Since the stochastic beam ions can travel all over an accessible region and thus are gradually lost from the mirror end throat or wall surface, the definition of beam ion confinement time is indispensable to estimate effects of NB injection. Recently, using a Monte Carlo code, Lifschitz *et al.* showed numerically the driven current, power and momentum transferred to FRCs by NB injection.[14] In their equilibrium model, the Grad-Shafranov equation is solved only inside the separatrix, and the approximated form is employed for the outer field. Therefore, the fast ion motion in the magnetic mirror field is difficult to discuss with their model. Furthermore, they calculated for the tangential NB injection (i.e., the beam path is perpendicular to the geometric axis) at the midplane; injection geometry is the same as the ARTEMIS design and different from the FIX's arrangement. Since an experimental report on tangential NB injection is unavailable so far, a comparison with experimental results is impossible and validity of numerical calculation is never estimated. In the present paper, a numerical computation of beam ion motion in the FRC equilibria with different mirror ratio, which is similar to the FIX experiment, is carried out to show a non-adiabaticity exhibited in the NB injected fast ion motion; it causes a deleterious orbit loss on the wall surface even if we apply the strong magnetic mirror field to reduce the end loss. A detailed analysis with respect to rapid changes of magnetic moment due to non-uniformity of FRC plasma is provided.

The organization of this paper is as follows. In Sec. II, we will describe our calculation model and explain the beam ion loss criteria using the concept of accessible region. Results from the numerical calculations of the particle motion and discussion on the beam ion loss due to the adiabaticity breaking process of beam ion motion are presented in Sec. III. Section IV is devoted to summarize conclusions.

II. COMPUTATIONAL MODEL

The calculation is carried out in order to compare with the NB injection experiment on the FIX device. The computational model of NB injection into the FRC is schematically drawn in FIG. 1. The NB particle goes along the direction of diamagnetic plasma current; it is the positive direction along the azimuthal coordinate in the present case. The NB is injected at an angle of ϕ toward the geometric axis (i.e., the z-axis), and it is shifted from the axis by a length b. Although in the FIX experiment the NB particles are dispersed in the Gaussian distribution around the beam axis,[7] a straight and non-dispersed beam path is assumed in the present calculation. To discuss the effect of the injection angle ϕ on the beam ion confinement, three typical injection angles are applied. Parameters used here are shown in TABLE I. These parameters are almost the same as those of the experimental setup on the FIX device except the length of the confinement region (1.8 m for the FIX case).

A. Ionization of neutral beam

NB particles are ionized by the following three processes:

1) the charge exchange,
2) the direct ionization due to an impact of a plasma particle (i.e., an ion or an electron),
3) the indirect ionization through the excitation processes.

The dominant ionization process is the charge exchange. In order to consider the excitation process, a two-step calculation is necessary, which complicates the calculation. Moreover, since the cross-section of excitation process is much smaller than others, therefore we neglect this: the charge exchange and direct ionization process are taken into account in the present calculation. The interactions between plasma particles and beam particles are calculated by a use of the Monte Carlo method. In this scheme, an ionization event takes place when the inequality

$$n\sigma(v_r)v_r\Delta t \geq \xi \qquad (1)$$

is satisfied. Here, the quantities n and v_r are the number density for a species of impacting particle, such as plasma ions, and the absolute value of relative velocity between an NB particle and the impacting plasma particle, respectively. The total ionization cross-section σ equals $\sigma_{ce}+\sigma_{di}$, where σ_{ce} and σ_{di} are the charge exchange cross-section and the direct ionization cross-section, respectively. The experimental data for σ_{ce} between a hydrogen atom and its ion (including the pair of deuterium atom and deuterium ion) is chosen from Refs. 15-24 and those of σ_{di} are cited from Refs. 17 and 25-27 for the ion impact and Refs.28-31 for the electron impact. The impact energy dependence of cross-section is expressed by several analytical curves; each of them is given in an appropriate energy range so as to fit well to the experimental data. The time interval Δt for generation of random numbers is short enough that the value $n\sigma(v_r)v_r\Delta t$ is less than unity and is long enough to reduce the calculation time. Thus we choose

$$\Delta t = \frac{0.01}{n_{\mathrm{null}}\sigma_0 v_{\mathrm{NB}}},$$

where n_{null}, σ_0, and v_{NB} are the number density at the field-null O-point, the reference cross-section (i.e., 1.0×10^{-19} m^2 that nearly equals the value of σ_{ce} at the impact energy of 10 keV), and the speed of NB particle. The uniform random number ξ is generated by the M-sequence[32], which supplies a good uniformity to generate the random numbers.

B. Equilibrium

The density n, which is used in the inequality (1), is estimated from the total pressure $p = n_e T_e + n_i T_i = 2nT$, where T is the plasma temperature assumed to be uniform in the present study. The FRC equilibria are obtained by solving the Grad-Shafranov equation for the flux function ψ:

$$r\frac{\partial}{\partial r}\left(\frac{1}{r}\frac{\partial\psi}{\partial r}\right)+\frac{\partial^2\psi}{\partial z^2} = -\mu_0 r^2\frac{\mathrm{d}p}{\mathrm{d}\psi}. \qquad (2)$$

Using the symmetry $\psi(r,z)=\psi(r,-z)$, we solve Eq. (2) in $z\geq 0$. The pressure p as a function of ψ is given as follows:

$$p(\psi)=\begin{cases} a_0+a_1\psi+a_2\psi^2+a_3\psi^3 \equiv p_{\mathrm{in}}(\psi) & \psi\geq 0 \\ b_0\exp(b_1\psi)\equiv p_{\mathrm{out}}(\psi) & \psi<0 \end{cases}, \qquad (3)$$

where as and bs are coefficients which are set so as the current density and pressure at the separatrix to connect smoothly. Therefore, we apply the conditions:

$$p_{\mathrm{in}}(\psi=0)=p_{\mathrm{out}}(\psi=0),$$

$$\mathrm{d}p_{\mathrm{in}}/\mathrm{d}\psi\big|_{\psi=0}=\mathrm{d}p_{\mathrm{out}}/\mathrm{d}\psi\big|_{\psi=0},$$

$$\mathrm{d}^2p_{\mathrm{in}}/\mathrm{d}\psi^2\big|_{\psi=0}=\mathrm{d}^2p_{\mathrm{out}}/\mathrm{d}\psi^2\big|_{\psi=0}.$$

Also, we give the values of pressure at the separatrix and the wall. One degree of freedom remains to be specified, and this controls the equilibrium state. The flux function at the wall is given by

$$\psi(r_{\mathrm{w}},z)=\begin{cases}\psi_{\mathrm{w}} & 0\leq z\leq z_{\mathrm{c}} \\ \dfrac{R_\psi+1}{2}\psi_{\mathrm{w}}+\dfrac{1-R_\psi}{2}\psi_{\mathrm{w}}\cos\left(\dfrac{z-z_{\mathrm{c}}}{z_{\mathrm{mir}}-z_{\mathrm{c}}}\pi\right) & z>z_{\mathrm{c}}\end{cases} \qquad (4)$$

Here, z_{mir} is the axial length from the midplane to the mirror end, i.e., the half length of the confinement region, z_{c} is the axial position at which the mirror field critically influences, and R_ψ is a control parameter for the mirror ratio defined by the form $R_\psi \equiv |\psi(r_{\mathrm{w}},z_{\mathrm{mir}})/\psi_{\mathrm{w}}|$. The flux function on the mirror end plane (i.e., $z=z_{\mathrm{mir}}$) satisfies $\partial\psi/\partial z=0$. An example of contour lines for the obtained flux function is shown in FIG. 2. In order to equate the obtained field strength with the experimental one, the flux function on the wall and midplane ψ_w is estimated here from the following relation that is used in the excluded flux analysis:

$$\psi_{\mathrm{w}}=\int_{r_{\mathrm{s}}}^{r_{\mathrm{w}}} rB_z\,\mathrm{d}r \approx \frac{B_{\mathrm{ex}}}{2}\left(r_{\mathrm{w}}^2-r_{\mathrm{s}}^2\right)=\frac{B_{\mathrm{ex}}r_{\mathrm{w}}^2}{2}\left(1-x_{\mathrm{s}}^2\right). \qquad (5)$$

Strictly, the magnetic field B_z is non-uniform in the vicinity of the separatrix. The non-uniformity, however, is concentrated in a thin edge layer. Thus an error arose from the above estimation is safely small. Moreover, in order for the pressure profile in the edge layer to coincide with the experimental results from the FIX device seen in Ref. 33, the separatrix beta value and width of edge layer on the midplane are set to 0.53 and 8 cm respectively.

C. Beam ion motion

After suffering from the ionization process, the NB particles then become high-energy beam ions and start a gyrating motion. The kinetic energy $K = (1/2)mv^2$ and canonical angular momentum $P_\theta = mv_\theta r + q\psi$ are determined by the initial position and velocity at the instance of ionization. These two quantities are constants of motion in the axisymmetric FRC without the electric field and at a steady state. With a use of the two constants of motion, beam ion accessibility is restricted in the region where the inequality

$$K \geq U(r,z) = \frac{(P_\theta - q\psi(r,z))^2}{2mr^2} \qquad (6)$$

is satisfied, where $U(r,z)$ is the effective potential known as the Störmer potential[34]. This region is referred to as the "accessible region"[12, 13, 35]. The NB particles are assumed to be mono-energetic in the present study, and then the values of K are the same for all the test beam ions. On the other hand, the values of P_θ are distributed, because the initial azimuthal velocity v_θ and both the position and flux function ψ are determined randomly by the probabilistic ionization process. Therefore, the accessible regions are different among every test particles. The accessible region can be used for estimation of the confinement of fast ions. If the region is open to the mirror throat, the particle is able to travel to the mirror point. Thus it may sometimes suffer from *the end loss*. Let us describe the end loss criterion. The radial position $r_{\min}$ of the bottom for the effective potential $U(r,z)$ on the mirror end plane (i.e., $z = z_{\mathrm{mir}}$) is the solution to

$$-r\frac{\partial\psi}{\partial r}\bigg|_{z=z_{\mathrm{mir}}} = P_\theta/q - \psi(r, z_{\mathrm{mir}}). \qquad (7)$$

Note that we consider the case that $\psi \geq 0$ inside the separatrix. The end loss criterion is then written

$$K \geq \frac{(P_\theta - q\psi(r_{\min}, z_{\mathrm{mir}}))^2}{2mr_{\min}^2}. \qquad (8)$$

The beam ions with the accessible region contacting with the wall may also suffer from *the wall loss*. The wall loss criterion is

$$\frac{\sqrt{2mK}}{|q|} r_w \geq P_\theta/q - \psi_w. \qquad (9)$$

Therefore, depending on the two constants of motion K and P_θ, the shape of accessible region is found to be open or close at the mirror point toward outside the confinement system and to be contacting or not to be contacting with the wall. Four typical calculated accessible regions of fast ions are presented in FIG. 3. An ion with high K but small P_θ has two loss channels, the end and wall loss, as seen in FIG. 3 (a). An ion with lower K and the same P_θ as the case of FIG. 3 (a) becomes to have only the end loss channel. On the other hand, an ion with a positive and large P_θ is inaccessible to the mirror point [see FIG. 3 (c & d)].

The loss criteria described in Eqs. (8) and (9) are valid for perfectly stochastic ions (i.e., the ergodic ions). However, a beam ion with the open accessible region is not always lost because of the adiabatic motion and mirror confinement. Therefore, it is necessary to calculate the orbit of beam ion for a detailed discussion. An NB injected fast ion orbit is traced by a numerical integration of equation of motion:

$$m\frac{d\mathbf{v}}{dt} = q(\mathbf{v}\times\mathbf{B}). \qquad (10)$$

The electrostatic field is neglected in the present calculation. We employ the Adams method for the numerical integration of Eq. (10).

Suppose that a beam ion exhibits regular, integrable, or adiabatic behavior and does not strike against the wall before the first bounce at the magnetic mirror. It can be confined even in the case of the open or wall contacting accessible region. We showed that plasma ions in the edge region of FRC, however, suffer from the adiabaticity breaking process at the vicinity of field-null x-points.[12, 13] The magnetic moment $\mu = (1/2)mv_\perp^2/B$ jumps abruptly as it passes through the x-points, and is changed to another nearly constant value. We also showed in Ref. 35 that plasma ions confined inside the separatrix tend to be in a stochastic motion. Therefore, observation of the magnetic moment and a study for statistical properties of the abrupt change of magnetic moment are important to show the beam ion confinement and estimate the effects of NB injection on

heating and current drive, etc.

III. RESULTS AND DISCUSSION

Following the explanation of computational procedure, the calculation of position and velocity at an instance of ionization of NB particle is carried out. Then, we will be able to discuss confinement of the beam ions using the concept of accessible region. Assuming the ergodic orbits, we classify the loss channels without the orbit calculation. For a detailed discussion on adiabaticity in the beam ion motion, orbits of the beam ions are calculated.

A. Ionization

We compute the ionization process of NB particles by the Monte Carlo method. The number of test particles is 10,000, which is many enough to reduce a statistical error. Injection beam energies are 3 and 10 keV in the present case. More general specification of energy is to use a normalized energy. When $K_0 \equiv q^2 |\psi_w|^2 / (m r_w^2)$ is chosen as the reference value of energy, the normalized energies, K / K_0, are 0.707 for 3 keV and 2.36 for 10 keV, where the flux function on the wall and midplane $|\psi_w|$ is easily transformed into the external magnetic field B_{ex} with the aid of Eq. (5). The values in Eq. (5), B_{ex}, r_w and x_s, are 0.05 T, 0.4 m and 0.58, respectively. In FIG. 4 for 3 keV and FIG. 5 for 10 keV, the histograms of the number of test NB particles N with respect to the beam path length s, the flux function ψ, the canonical angular momentum P_θ, and the azimuthal velocity v_θ are shown in order to find a detail of interaction between NB and plasma particles and to find the initial condition of the beam ion motion.

It appears from FIGs. 4(d) and 5(d) that large fraction of particles is ionized when they carry the largest azimuthal velocity. Therefore, the most frequent ionization occurs on the x-axis in FIG. 1, i.e., the most adjacent position to the geometric axis. The NB particles enter the separatrix inside at s of about 1.0 m and go out at s of about 1.8 m. Compared with the 10-keV particles, the 3-keV particles are ionized frequently before they reach the maximum ionization point. However, more than 50 % of 10-keV particles still remain after the maximum ionization point, because the ionization frequency is lower in higher impact energy range. Although we assume mono-energetic NB particles here, values of the canonical angular momentum are distributed as shown in FIGs. 4(c) and 5(c). Since the beam ion loss criteria given in Eqs. (8) and (9) depend on the value P_θ, the distribution of P_θ gives the confined beam ion fraction with a use of the concept of accessible regions.

B. Accessible regions and velocity space particle loss of high energy ions

We described the loss criteria in Sec. II.C; they depend on the two constants of motion, the kinetic energy K and canonical angular momentum P_θ. As we described before, though K is a fixed value, values of P_θ are distributed: the distribution is determined by the condition at the instance of ionization. Therefore, the velocity space particle losses[36, 37] of fast ions can be found from Eqs. (8) and (9) without calculating an orbit of a fast ion. TABLE II shows the classification of confinement and losses of neutral beam injected fast ions, which is made using the criteria of Eqs. (8) and (9). The number of test particles is written in this table. It is found that both 3-keV and 10-keV ions suffer from orbit losses on the wall and also found that no fast ions are confined. Note that all the beam ions are lost, if they exhibit stochastic behavior in their motion. All the 3-keV ions are end lost at R_ψ of 2. However, the number of end loss ions decrease suddenly in the case that R_ψ=4. On the other hand, the sudden decrease is found for the 10-keV ions in the case that R_ψ=6. A higher mirror field is found to be effective to reduce the end loss; its effectiveness is dependent on the beam energy. On the contrary to the end loss, the wall loss is out of control by the mirror field; it is controllable only by the injection beam energy. It is necessary to use NB particles carrying less than 3-keV in order to suppress the wall loss. Suppose that the values of P_θ range from 0.1 to 0.2 as shown in FIG. 5 (c). Using the criterion of Eq. (9), we find that the NB injection less than 2.3-2.7 keV energy is needed for confinement of fast ions in the FIX's case.

C. End and wall losses due to adiabaticity breaking processes

Varying the value of R_ψ, i.e., changing the mirror ratio, we calculated various FRC equilibria so as to show confinement dependences of fast ions on the mirror ratio. Single particle orbits in prescribed FRC equilibria are calculated. Initial conditions of the calculation are given from the results of ionization processes by the Monte Carlo method. Numerical error of the integration is checked using a conservation of two constants of motion, K and P_θ. The deviations

$$\varepsilon_K \equiv \frac{K(t)-K(0)}{K(0)}, \quad \varepsilon_{P\theta} \equiv \frac{P_\theta(t)-P_\theta(0)}{P_\theta(0)}$$

are less than 10^{-10} for all cases, which are small enough to obtain reliable results. Figure 6 shows the typical orbits of (a) 3-keV and (b) 10-keV fast ions in the FRC equilibrium with R_ψ of 10. Radial extent for 10-keV fast ion orbit is apparently wider than for the 3-keV ion. In the present case, however, the 3-keV ion goes into the mirror region deeper. It is found visually that the 10-keV ion at last suffers from the orbit loss on the wall. On the other hand, the 3-keV ion is confined up to the end of the orbit calculation time $t\omega_{ci} = 100$, where $\omega_{ci} \equiv q|\psi_w|/mr_w^2$. Both the 10-keV and 3-keV ions are found to bounce axially several times in the mirror region. Also, one can find easily that the ions cross frequently the separatrix. This implies that the fast ions often feel a sharp variation of the magnetic field. Adiabaticity of plasma particle motion originates in the negligible change of the magnetic field in one cyclotron motion. Fast ions in FRCs, however, travel in the non-uniform field, and thus are subject to adiabaticity breaking processes. Observation of the magnetic moment can show clearly the processes. Time evolutions of the magnetic moment are presented in FIG. 7(a) for the 3-keV ion and FIG. 8(a) for the 10-keV ion, and the synchronous flux function (b) and positions (c) are also presented. The magnetic moment jumps when the fast ion crosses the separatrix or passes near the x-points. This is because non-uniformity of the magnetic field is considerable inside the separatrix rather than outside the separatrix except in the vicinity of the x-points. Therefore, we might consider that an FRC is a source of the non-adiabatic motion of the fast ions.

Because of the non-adiabatic motion of fast ions, these ions are lost gradually on the wall surface or from the mirror point. Figure 9 shows that the confined fast ion fraction in percentage α observed at their each mirror reflection. The injection angle is the same as the FIX experiment (i.e., 19.3°). Here, N_M stands for the number of mirror reflection. Injection beam energies are (a) 3, (b) 10 and (c) 14 keV. The mirror reflection is defined here as

$$v_\parallel(t+\Delta t)\cdot v_\parallel(t) < 0 \quad \text{and} \quad \psi(t+\Delta t) < 0,$$

where Δt is the time interval for numerical integration of the equation of motion. Except for the case of R_ψ of 2, the 3-keV ions are confined well till $N_M = 10$. For higher energy NB injection as shown in FIG. 9(b) and (c), however, the confined fraction α decreases for every value of R_ψ. Less than 10 % of fast ions remain in the confinement system at $N_M = 10$.

One can find that for the 10-keV ions the best confinement is not in the case of $R_\psi = 10$ but $R_\psi = 8$. This suggests that the effects of mirror field on the 10-keV beam ion confinement are saturated at $R_\psi = 8$. Accessible regions of 10-keV ions become close at the mirror points for the case that $R_\psi = 8$ and 10 as shown in FIG. 3 (c). Therefore, a stronger magnetic mirror than $R_\psi = 8$ is ineffective to the suppression of the end losses. On the other hand, the wall loss on the midplane is independent of the magnetic mirror, because the criterion Eq. (9) is independent of the magnetic mirror. Therefore, for the case of R_ψ of both 8 and 10, the end loss is completely suppressed and the difference between them arises from the frequency of the wall loss. The result of larger α for $R_\psi = 8$ and 10-keV ions shown in FIG 9(b) implies that the number of wall loss ions due to orbit deflection by adiabaticity breaking processes is lesser for the case of R_ψ of 8 than for 10. The frequency of the wall loss may depend on the magnetic structure and statistical property of the beam ion motion.

In order to clarify the non-adiabatic motion of beam ions, we observe the correlations of the magnetic moment at the mirror reflection. The results are shown in FIG. 10. Since the

magnetic moment keeps nearly constant around the mirror reflection point [see FIGs. 7 and 8], the point is chosen for observation of the magnetic moment in the present study. The horizontal axis of each figure is the magnetic moment at the first mirror reflection μ_1, and the vertical axis is the one at (a)(b) the second μ_2, (c) (d) the third μ_3, and (e) (f) the fourth μ_4 of the reflection. The 3-keV ions are shown in FIGs. 10 (a), (c) and (e) and the 10-keV ions are shown in FIGs. 10 (b), (d) and (f). Note that if the magnetic moment is conserved completely, the plotted points should be on the straight line $\mu_1 = \mu_2, \mu_3$, and μ_4. If μ_1 correlates with μ_2, μ_3, and μ_4, the neighboring points in μ_1 are plotted also at the neighboring points in μ_2, μ_3, and μ_4. Consequently, if the magnetic moments are correlated, we can see a series of correlated points visually as a connected curve; it is shown as a waving curve in FIGs. 10(a), (c), and (e) for the case of 3-keV ions, and in FIG. 10 (a) alone for 10-keV ions. On the other hand, the waving curve disappears in FIG. 10 (d) and (f) for the 10-keV ions, and thus the correlation of the magnetic moment vanishes because of the adiabaticity breaking processes. Due to this perfect stochastization, the fast ion orbits become ergodic. Therefore, the loss criteria Eqs. (8) and (9) by the concept of accessible regions are valid. Note that no confined beam ions are found in TABLE II for the injection beam energy of 10 keV. This result is consistent with the fact $\alpha \to 0$ as N_M increases as shown in FIG. 9. In Ref. 6, the trapped fraction of beam ions are shown, where more than 60% of beam ions have been found to be trapped. This result is different from the present one. The difference may arise from the condition to judge the confinement of beam ions. The trapped duration time of beam ion may be different, although no definite description of the trapped duration time of trap is provided in Ref. 6.

Dependency of the confined beam ion fraction α on the injection angle ϕ is also examined. This study supplies a proposal for more effective NB injection. The two other injection angles are chosen: for the case that $\phi = 8.09$, the beam is directed toward the field-null O-point (i.e., the magnetic axis), and for the case that $\phi = 11.3$, the beam is directed toward the center of confinement region (i.e., $r = 0$ and $z = 0$). The confined 14-keV ion fraction α is shown in FIG. 11. For both the injection angle of (a) 8.09° and (b) 11.3°, α decreases more rapidly than for the case of 19.3° in FIG. 9 (c). The current experimental setup of NB injection on the FIX device is found to be more effective than our prametric choice.

To make a comparison of the current result with the experiment carried out on the FIX device, let us define a dimensionless effectiveness parameter. The ensemble averaged number of the axial one-way motion until the beam ions are lost are calculated as

$$\langle N_t \rangle = \sum_{N_M=1}^{10} N_M \frac{\alpha(N_M - 1) - \alpha(N_M)}{100}.$$

If we assume the effects of the NB injection is proportional to the averaged trapped duration of beam ions, we can estimate the effectiveness of NB injection qualitatively by the value of $\langle N_t \rangle$. The comparison with the experimental results reported in Ref. 6 is made in FIG. 12. To compare with Ref. 6, R_ψ should be transformed into the customary mirror ratio R_M. Assuming a uniform magnetic field both on the midplane and outside the separatrix B_0 and on the mirror end throat B_M, the customary mirror ratio $R_M \equiv B_M / B_0$ is $R_M = (1 - x_s^2) R_\psi$. Typical x_s in our calculation is about 0.58, then $R_M \approx 0.67 R_\psi$. The mirror ratio dependence on $\langle N_t \rangle$ for 10- and 14-keV ions and the ratio of the configuration life time τ_V with and without NB injection shown in Ref. 12 are presented. The beam energy is 14 keV in the case of Ref. 12. The effectiveness parameter $\langle N_t \rangle$ for 10- and 14-keV ions are gradually increased as the mirror ratio goes higher. The value of $\langle N_t \rangle$ for 10-keV, however, is saturated at $R_M \approx 5$. It seems that $\langle N_t \rangle$ keeps rising in $R_M \geq 7$. From this figure, a higher magnetic field is found to be more effective to trap the fast ions, although they are lost on the wall eventually. The degree of its effectiveness is, however, dependent on the beam energy. The sudden increase of the effect of NB injection is observed experimentally at $R_M = 8$; it may be resulted from a nonlinear electromagnetic effect. It is difficult to explain the abrupt increase in improvement of confinement at $R_M \approx 8$ by the present analysis. A self-consistent electromagnetic and

beam ion kinetic model is needed to predict an experimental behavior.

IV. CONCLUSIONS

The neutral beam (NB) injection into the Field-Reversed Configuration has been analyzed numerically. The calculation parameters are relevant to the NB injection experiment on the FIX device. Ionization processes of beam particles are calculated by the Monte Carlo method. Ionization through the charge exchange processes is found to be dominant: 85 % for 3 keV and 80 % for 10 keV beam energy. The accessible regions that are determined from the two constants of motion, the kinetic energy and the canonical angular momentum, have been calculated to give the loss criteria. The neutral beam injected fast ions have two loss channels: the loss on the surface of the wall (the wall loss), and/or the loss from the mirror end point (the end losses). With a use of the loss criteria derived by the shape of accessible region, no fast ions are found to be confined for the beam energy of 10 keV. It is found that the end loss is suppressed by the strong mirror field and the wall loss channel however still exists. The loss criteria by the accessible regions are based on the assumption of the non-adiabatic motion and ergodic orbits for the beam ions. For a detailed discussion, single particle orbits have been calculated to show an adiabaticity or non-adiabaticity exhibited in the beam ion motion. The magnetic moment is found to be changed stochastically near and/or inside the separatrix. Moreover, the calculation of the correlation of magnetic moment at several instances of mirror reflection shows clearly the non-adiabaticity of beam ion motion. Therefore, the loss criteria by the shape of the accessible region are found to be valid, unless we consider the trapped duration time of beam ions. It is found from the single particle orbit calculation that the trapped fraction of beam ions is gradually decreased as they experience the mirror reflection. It occurs even in the case of a strong mirror field, because the wall orbit loss is never suppressed by the mirror field. Although the strong dependence of effectiveness of the neutral beam injection on the mirror ratio reported in the FIX experiment is also observed in the present calculation, however, a detailed analysis on such as the power deposition, heating, current drive, and stabilization, remains to be carried out in a near future.

ACKNOWLEDGEMENTS

One of the authors (T. T) wishes to acknowledge valuable discussions via e-mail with Dr. Inomoto Michiaki at Osaka University. This work is performed with the support and under the auspices of the NIFS Collaborative Research Program.

[1] M. Tuszewski, Nucl. Fusion **28**, 2033 (1988).

[2] W. T. Armstrong, R. K. Linford, J. Lipson, D. A. Platts, and E. G. Sherwood, Phys. Fluids **24**, 2068 (1981).

[3] H. Momota, A. Ishida, Y. Kohzaki, G. H. Miley, S. Ohi, M. Ohnishi, K. Sato, L. C. Steinhauer, Y. Tomita, and M. Tuszewski, Fusion Technol. **21**, 2307 (1992).

[4] H. Momota, O. Motojima, M. Okamoto, S. Sudo, Y. Tomita, S. Yamaguchi, A. Iiyoshi, M. Onozuka, M. Ohnishi, and C. Uenosono, Proceedings of the Seventh International Conference on Emerging Nuclear Energy Systems, Makuhari, Chiba 1993 (World Scientific, Singapore, 1993) p. 16.

[5] A. Shiokawa and S. Goto, Phys. Fluids B **5**, 534 (1993).

[6] T. Asai, Y. Suzuki, T. Yoneda, F. Kodera, M. Okubo, S. Okada, and S. Goto, Phys. Plasmas **7**, 2294 (2000).

[7] T. Asai, Ph.D. thesis, Graduate School of Engineering, Osaka University, Japan, 2001.

[8] T. Asai, F. Kodera, M. Okubo, S. Okada, and S. Goto, J. Plasma Fusion Res. **77**, 1230 (2001).

[9] S. Okada, T. Asai, F. Kodera, K. Kitano, Y. Suzuki, K. Yamanaka, T. Kanki, M. Inomoto, S. Yoshimura, M. Okubo, S. Sugimoto, S. Ohi, and S. Goto, Nucl. Fusion **41**, 625 (2001).

[10] T. Asai, M.Inomoto, N. Iwasawa, S. Okada, and S. Goto, Phys. Plasmas **10**, 3608 (2003).

[11] M. Inomoto (private communication, Sep. 2002).

[12] T. Takahashi, Y. Tomita, H. Momota, N. V. Shabrov, Phys. Plasmas **12**, 4301 (1997).

[13] T. Takahashi, Ph.D. thesis, Dept. Fusion Science, The Graduate University of Advanced Studies, Japan, 1997.

[14] A. F. Lifschitz, R. Farengo, and N. R. Arista, Nucl. Fusion **42**, 863 (2002).

[15] V. A. Belyaev, B.G. Brezhnev, and E.M. Erastov, Sov. Phys. -JETP **25**, 777 (1967).

[16] W. L. Fite, R. T. Brackmann, and W. M. R. Snow, Phys. Rev. **112**, 1161 (1958).

[17] W. L. Fite, R. F. Stebbings, D. G. Hummer, and R. T. Brackmann, Phys. Rev. **119**, 663 (1960).

[18] J. E. Bayfield, Phys. Rev. **185**, 105 (1969).

[19] W. L. Fite, A. C. Smith, and R. F. Stebbings, Proc. Roy. Soc. A **268**, 527 (1962).

[20] H. B. Gilbody and G. Ryding, Proc. Roy. Soc. A **291**, 438 (1966).

[21] A. B. Wittkower, G. Ryding, and H. B. Gilbody, Proc. Phys. Soc. **89**, 541 (1966).

[22] G. W. McClure, Phys. Rev. **148,** 47 (1966).

[23] J. H. Newman, J. D. Cogan, D. L. Ziegler, D. E. Nitz, R. D. Rundel, K. A. Smith, and R. F. Stebbings, Phys. Rev. A **25**, 2976 (1982).

[24] P. Hvelplund and A. Andersen, Physica Scripta **26**, 375 (1982).

[25] H. B. Gilbody and J. V. Ireland, Proc. Roy. Soc. A **277**, 137 (1964).

[26] J. T. Park, J. E. Aldag, J. M. George, and J. L. Peacher, Phys. Rev. A **15**, 508 (1977).

[27] M. B. Shah and H. B. Gilbody, J. Phys. B **14**, 2361 (1981).

[28] W. L. Fite and R. T. Brackmann, Phys. Rev. **112,** 1141 (1958).

[29] E. W. Rothe, L. L. Marino, R. H. Neynaber, and S. M. Trujillo, Phys. Rev. **125**, 582 (1962).

[30] J. W. McGowan and E. M. Clarke, Phys. Rev. **167**, 43 (1968).

[31] M. B. Shah, D. S. Elliott, and H. B. Gilbody, J. Phys. B **20**, 3501 (1987).

[32] M. Fushimi, *Random number* (Japanese title is "Ran-Suu") (University of Tokyo Press, 1989, ISBN 4-13-064072-0) (in Japanese).

[33] T. Ohtsuka, M. Okubo, S. Okada, and S. Goto, Phys. Plasmas **5**, 3649(1998).

[34] C. Störmer, *The Polar Aurora* (Oxford University Press, 1955).

[35] Y. Hayakawa, T. Takahashi, Y. Kondoh, Nucl. Fusion **42**, 1075 (2002).

[36] M. –Y. Hsiao and G. H. Miley, Nucl.. Fusion **24**, 1029 (1984).

[37] M. –Y. Hsiao and G. H. Miley, Phys. Fluids **28**, 1440 (1985).

Tables

Table I. Geometry, plasma, and NB parameters.

Parameters	Symbols	Values
Incident angle	ϕ	8.09, 11.3 and 19.3 degree
Impact parameter	b	0.1 m
Beam energy	E_b	3 , 10, and 14 keV
External magnetic field	B_{cx}	0.05 T
Plasma temperature	$T=T_i+T_e$	150 (100+50) eV
Number density at O-point	n	5.0×10^{19} m^3
Wall radius	r_w	0.4 m
Half length of confinement region	z_{mir}	2.0 m

Table II. Classification of ionization processes of NB particles and of confinement and losses of fast ions.

	3 keV					10 keV				
R_{ip}	2	4	6	8	10	2	4	6	8	10
Charge exchange	8,510	8,582	8,479	8,457	8,480	7,973	7,938	7,886	7,901	7,906
Ionization by ions	13	10	16	14	10	602	651	662	628	644
Ionization by electrons	1,477	1,404	1,499	1,521	1,501	1,394	1,357	1,370	1,367	1,342
Total ionized particles A	10,000	9,996	9,994	9,992	9,991	9,969	9,946	9,918	9,896	9,892
Confined ions	0	0	0	0	0	0	0	0	0	0
End lost ions	0	0	0	0	0	0	0	0	0	0
Wall lost ions	0	7,102	7,984	8,410	8,523	0	0	6,476	8,343	8,918
End & wall lost ions	10,000	2,894	2,010	1,582	1,468	9,969	9,946	3,442	1,553	974
Wall striking particles B	0	4	6	8	9	31	54	82	104	108
Total test particles A+B	10,000	10,000	10,000	10,000	10,000	10,000	10,000	10,000	10,000	10,000

Figures

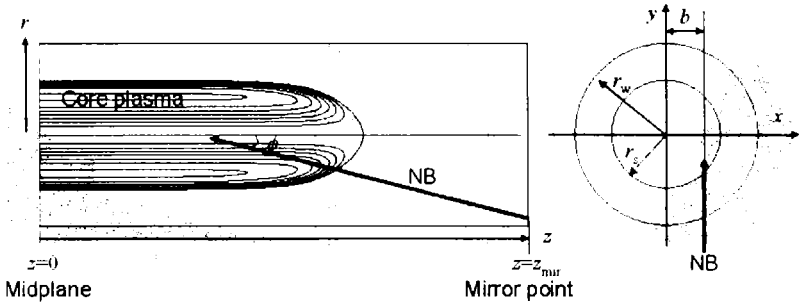

FIG. 1. Schematic view of NB injection geometry. A NB particle is injected obliquely at an angle of ϕ to the geometric axis and with an impact parameter of b.

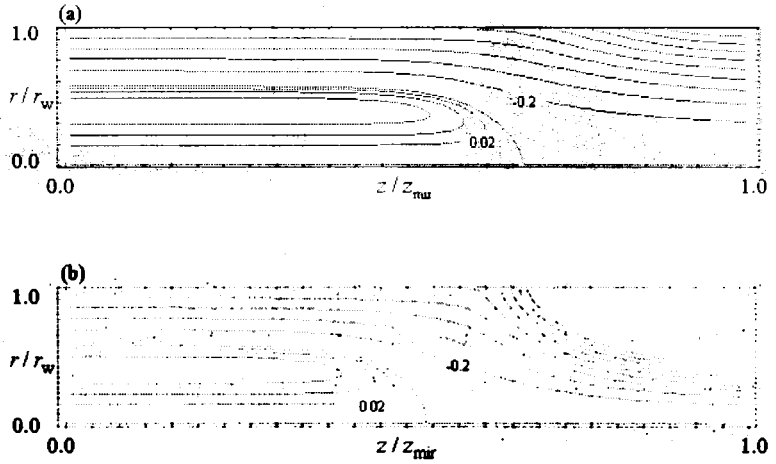

FIG. 2. The contour lines of the normalized flux function $\psi / |\psi_w|$ in the r-z plane for the case of (a) $R_\psi = 2$ and (b) $R_\psi = 10$. The contour intervals are 0.02 for inside the separatrix and 0.2 for outside the separatrix. The normalized separatrix radius $r_s / r_w = x_s$ is 0.58 for both and the normalized half length $(\ell_s / 2)/ z_{mir}$ is (a) 0.67 and (b) 0.53.

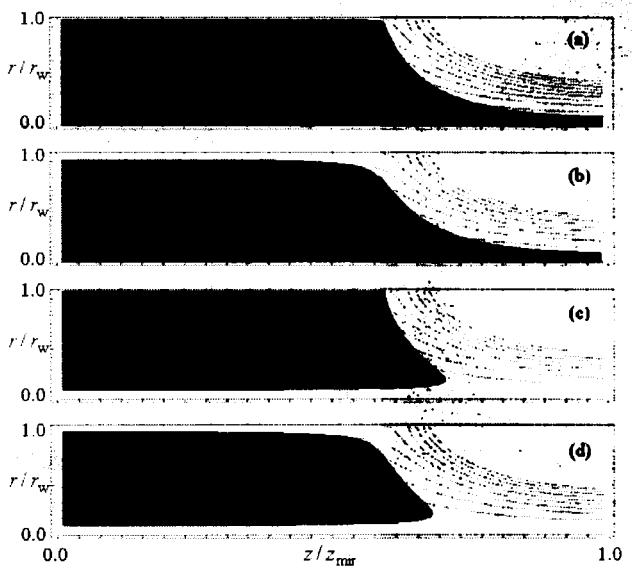

FIG. 3. Four typical accessible regions for relatively high-energy ions. The kinetic energy K and the canonical angular momentum P_θ are (a) $K / K_0 = 0.5$ and $P_\theta / P_{\theta 0} = 0.005$, (b) $K / K_0 = 0.4$ and $P_\theta / P_{\theta 0} = 0.005$, (c) $K / K_0 = 0.605$ and $P_\theta / P_{\theta 0} = 0.1$, and (d) $K / K_0 = 0.5$ and $P_\theta / P_{\theta 0} = 0.1$. The reference values for normalization, K_0 and $P_{\theta 0}$, are $K_0 \equiv q^2 |\psi_w|^2 / (m r_w^2)$ and $P_{\theta 0} \equiv q |\psi_w|$. The flux function on the wall and midplane $|\psi_w|$ is transformed into the external magnetic field B_{ex} with the aid of Eq. (5). In all the cases, $R_\psi = 10$.

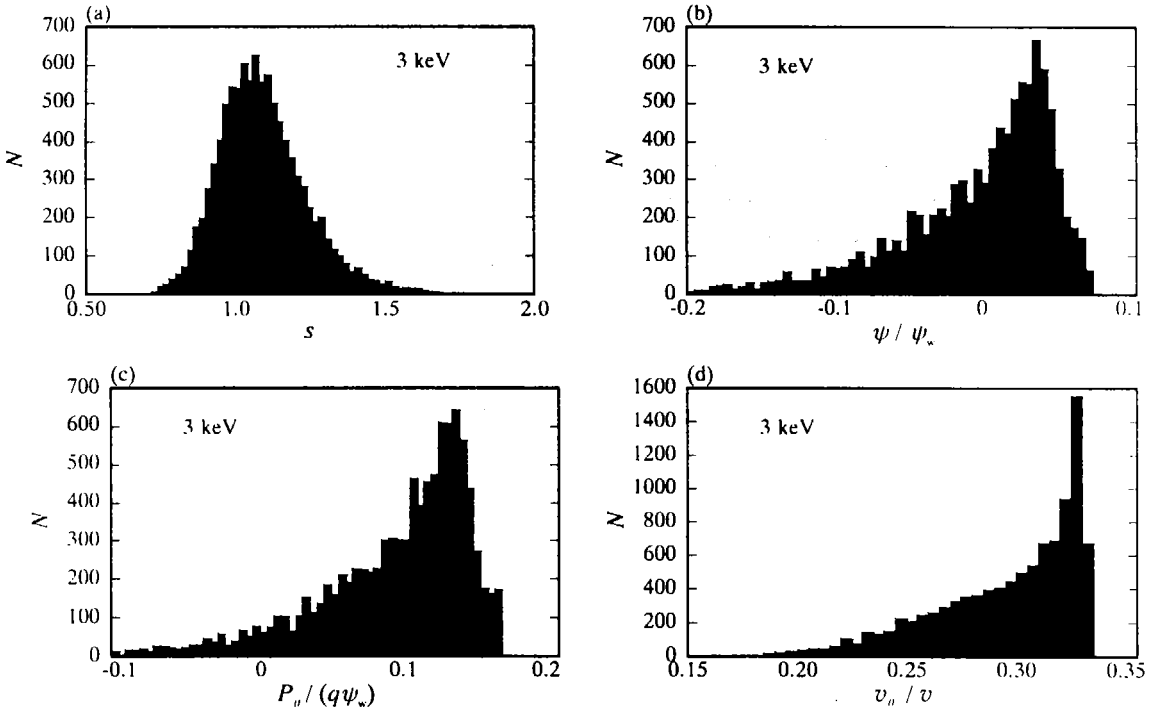

FIG. 4. The histograms of the number of 3-keV NB particles at the instance of the ionization. The horizontal axes are (a) the beam path length s from the NB injector, (b) the flux function ψ, (c) the canonical angular momentum P_θ, and (d) the fraction of the azimuthal velocity component to the absolute value of the velocity. The particles striking the wall before being ionized are omitted from this figure. In all the cases, $R_\psi = 10$.

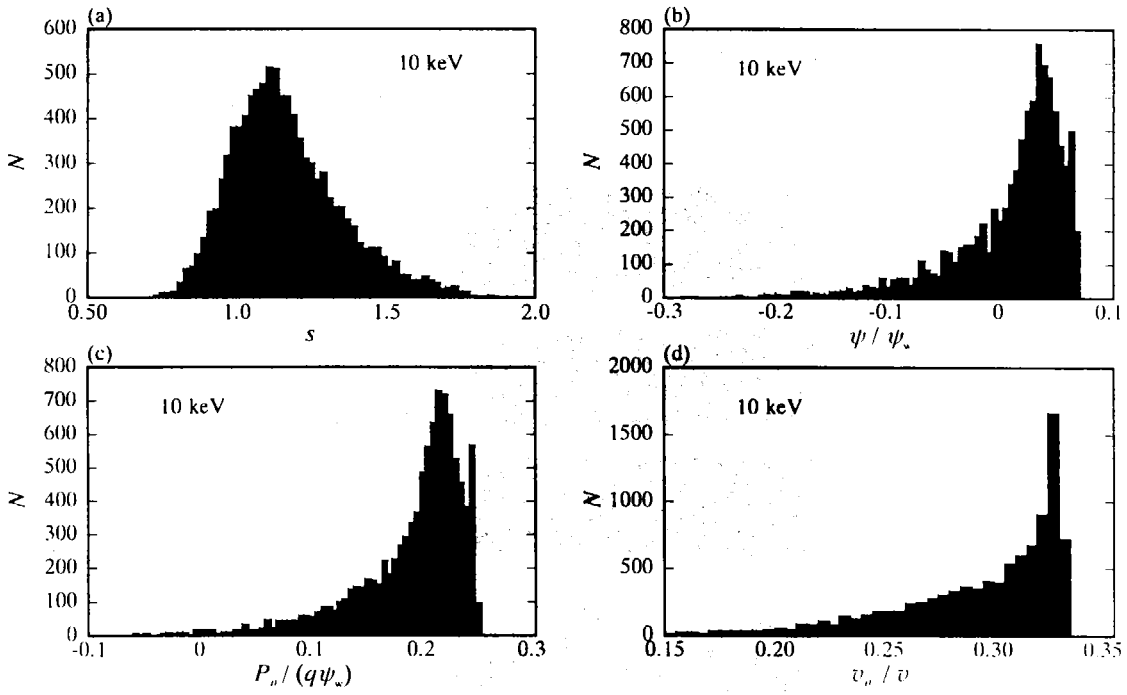

FIG. 5. The histograms of the number of 10-keV NB particles at the instance of the ionization. The horizontal axes are (a) the beam path length s from the NB injector, (b) the flux function ψ, (c) the canonical angular momentum P_θ, and (d) the fraction of the azimuthal velocity component to the absolute value of the velocity. The particles striking the wall before being ionized are omitted from this figure. In all the cases, $R_\psi = 10$.

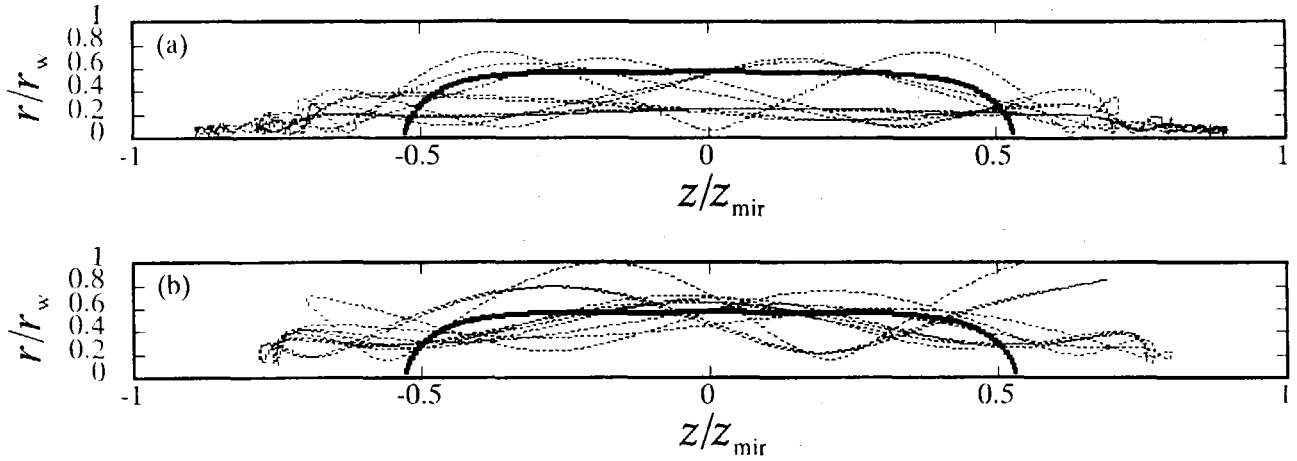

FIG. 6. Typical orbits of beam ion for (a) 3 keV and (b) 10 keV in the case of $R_\psi = 10$.

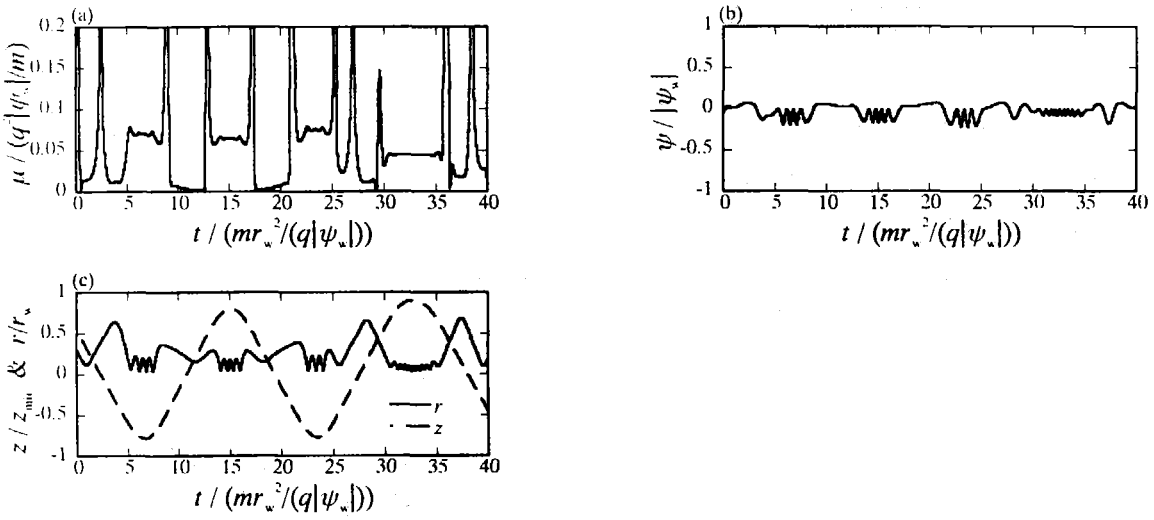

FIG. 7. Time evolutions of (a) the magnetic moment (b) the flux function (c) the axial position for the sample test beam ions in FIG. 6(a) with the energy of 3 keV.

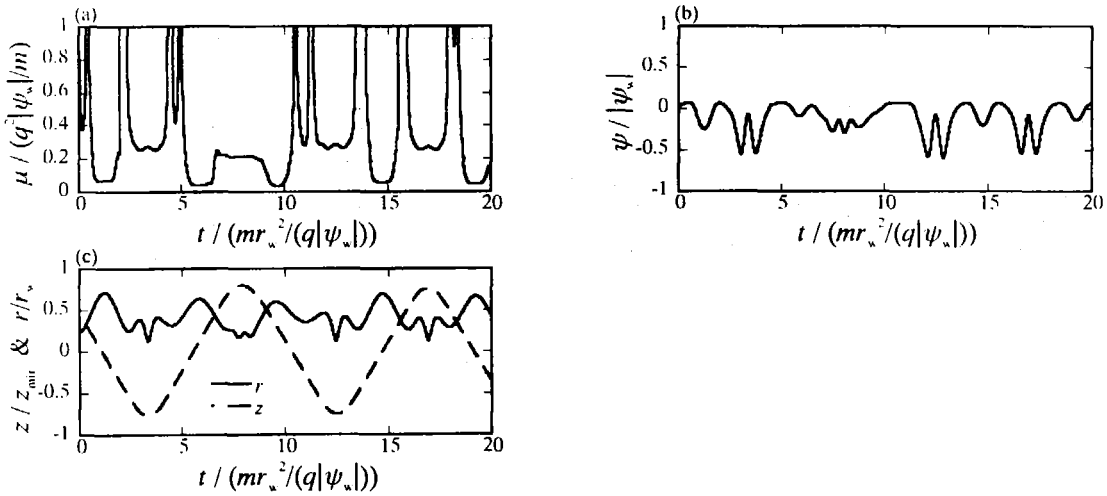

FIG. 8. Time evolutions of (a) the magnetic moment (b) the flux function (c) the axial position for the sample test beam ions in FIG. 6(b) with the energy of 10 keV.

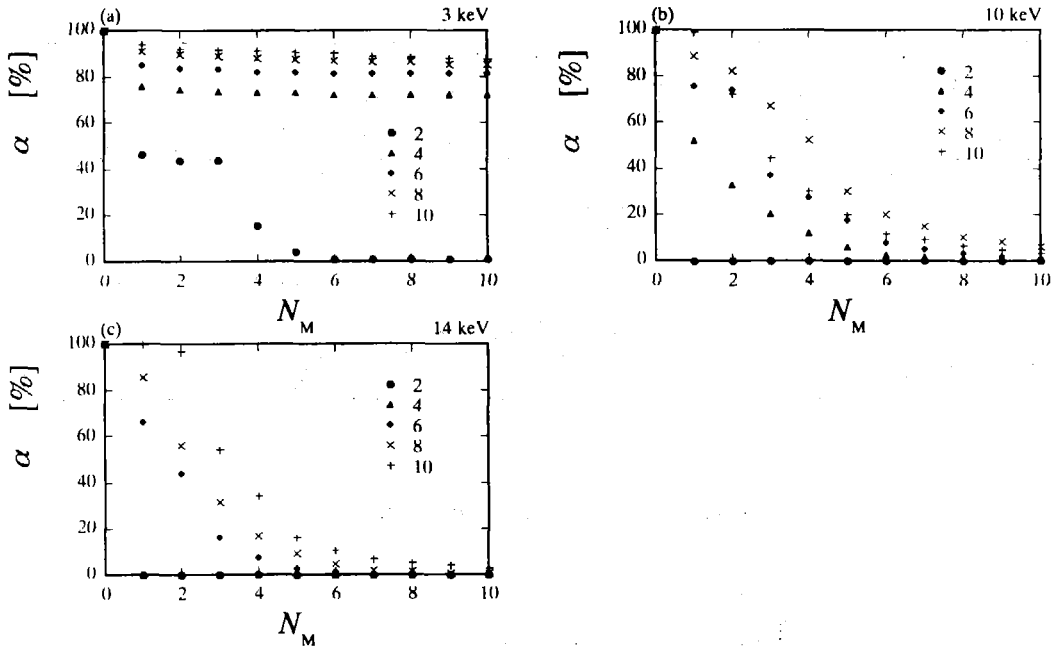

FIG. 9. Relation between confined fast ion fraction in percentage and the number of mirror reflection. Injection beam energies are (a) 3 keV, (b) 10 keV and (c) 14 keV. The values of mirror ratio control parameter R_ψ are 2 (solid circle), 4 (solid triangle), 6 (solid diamond), 8 (cross), and 10 (plus).

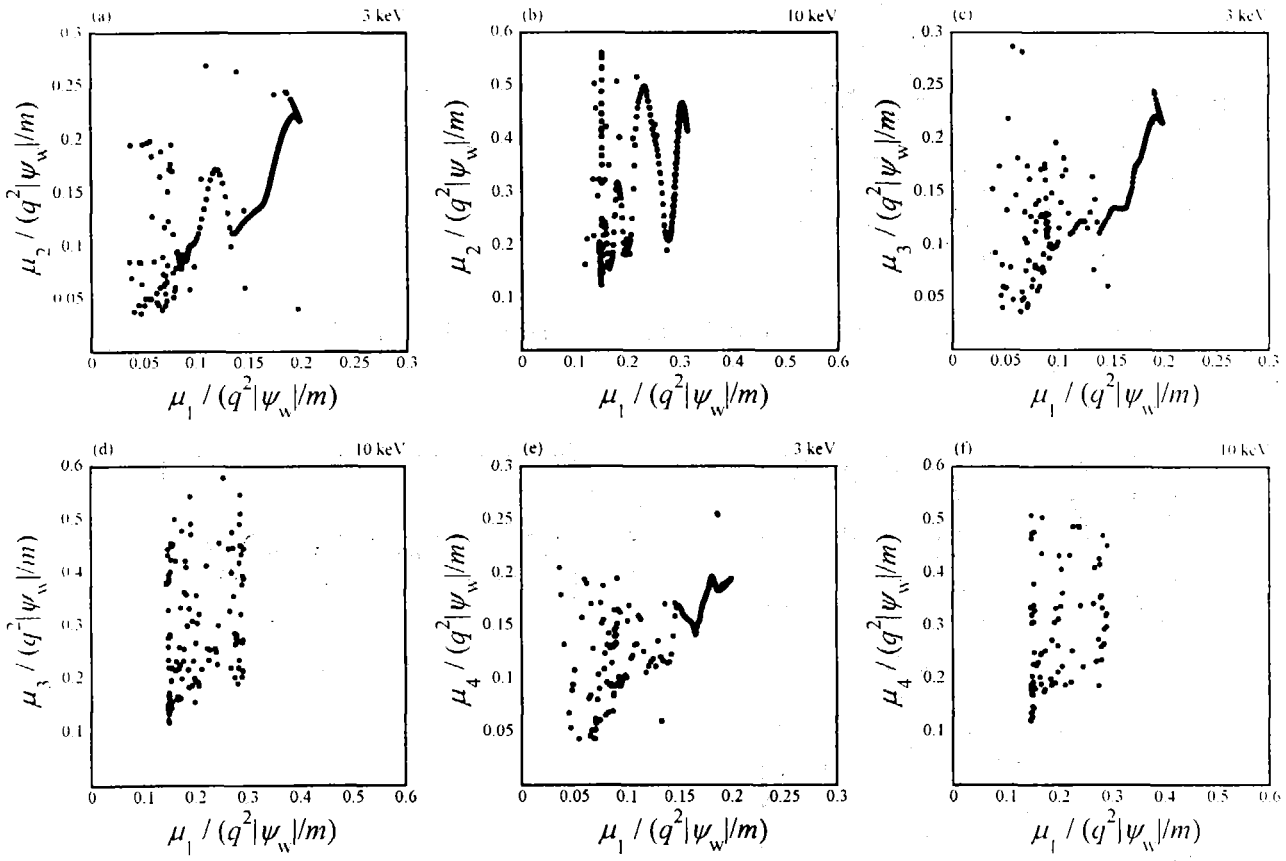

FIG. 10. The correlations of the magnetic moment between at the first mirror reflection and at (a)(b) the second, (c)(d) third, and (e)(f) fourth reflection. The injection beam energies are (a)(c)(f) 3 keV and (b)(d)(f) 10 keV. The magnetic moment μ is normalized by the quantity $q^2 |\psi_w| / m$.

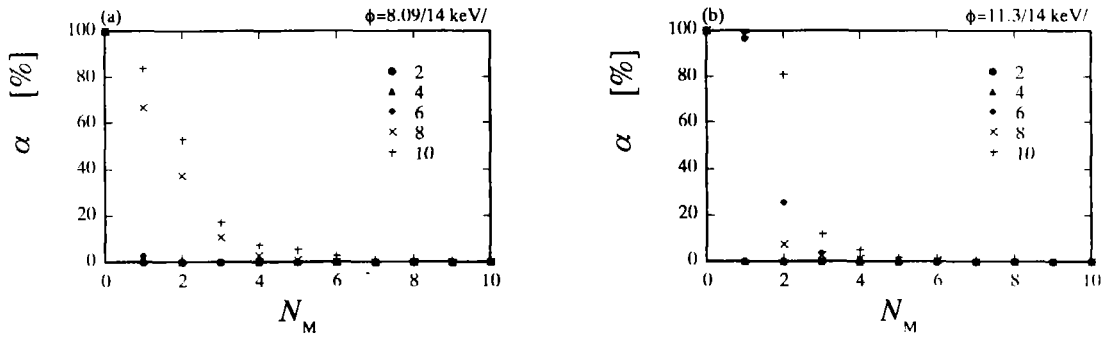

FIG. 11. Relation between confined fast ion fraction in percentage and the number of mirror reflection for injection beam energy of 14 keV. NB particles are injected obliquely to the geometric axis at an angle of (a) 8.09 and (b) 11.3 degree. The beam path is directed to the field-null O-point for the case (a) and to the center of confinement region (i.e., $r = 0$ and $z = 0$) for the case (b). The values of mirror ratio control parameter R_ψ are 2 (solid circle), 4 (solid triangle), 6 (solid diamond), 8 (cross), and 10 (plus).

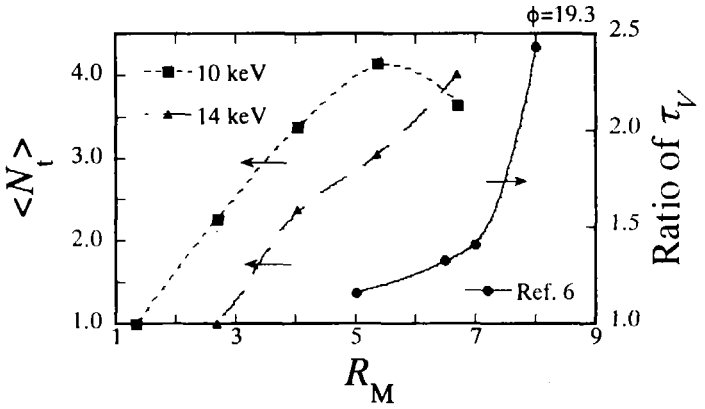

FIG. 12. Dependency of the ensemble averaged number of the axial one-way motion until the beam ions are lost $\langle N_t \rangle$ and the ratio of the configuration lifetime τ_V with and without the NB injection in Ref. 6 (solid circle) on the mirror ratio R_M. The injection energies are 10 keV (solid square) and 14 keV (solid triangle) for $\langle N_t \rangle$. The lines are drawn to guide the reader's eye.

Recent Issues of NIFS Series

NIFS-767 R. Kanno, N. Nakajima, M. Okamoto and T. Hayashi
Computational Study of Three Dimensional MHD Equilibrium with m/n=1/1 Island
Dec. 2002

NIFS-768 M. Yagi, S.-I. Itoh, M. Kawasaki, K. Itoh and A. Fukuyama
Multiple-Scale Turbulence and Bifurcaion
Jan. 2003

NIFS-769 S.-I. Itoh, K. Itoh and S. Toda
Statistical Theory of L-H Transition and its Implication to Threshold Database
Jan. 2003

NIFS-770 K. Itoh
Summary: Theory of Magnetic Confinement
Jan. 2003

NIFS-771 S.-I. Itoh, K. Itoh and S. Toda
Statistical Theory of L-H Transition in Tokamaks
Jan. 2003

NIFS-772 M. Stepic, L. Hadzievski and M.M. Skoric
Modulation Instability in Two-dimensional Nonlinear Schrodinger Lattice Models with Dispersion and Long-range Interactions
Jan. 2003

NIFS-773 M.Yu. Isaev, K.Y. Watanabe, M. Yokoyama and K. Yamazaki
The Effect of Hexapole and Vertical Fields on α-particle Confinement in Heliotron Configurations
Mar. 2003

NIFS-774 K. Itoh, S.-I. Itoh, F. Spineanu, M.O. Vlad and M. Kawasaki
On Transition in Plasma Turbulence with Multiple Scale Lengths
May 2003

NIFS-775 M. Vlad, F. Spineanu, K. Itoh, S.-I. Itoh
Intermittent and Global Transitions in Plasma Turbulence
July 2003

NIFS-776 Y. Kondoh, M. Kondo, K. Shimoda, T. Takahashi and K. Osuga
Innovative Direct Energy Conversion Systems from Fusion Output Thermal Power to the Electrical One with the Use of Electronic Adiabatic Processes of Electron Fluid in Solid Conductors.
July 2003

NIFS-777 S.-I. Itoh, K. Itoh and M. Yagi
A Novel Turbulence Trigger for Neoclassical Tearing Modes in Tokamaks
July 2003

NIFS-778 T. Utsumi, J. Koga, T. Yabe, Y. Ogata, E. Matsunaga, T. Aoki and M. Sekine
Basis Set Approach in the Constrained Interpolation Profile Method
July 2003

NIFS-779 Oleg I. Tolstikhin and C. Namba
CTBC A Program to Solve the Collinear Three-Body Coulomb Problem: Bound States and Scattering Below the Three-Body Disintegration Threshold
Aug. 2003

NIFS-780 Contributions to 30th European Physical Society Conference on Controlled Fusion and Plasma Physics (St.Petersburg, Russia, 7-11 July 2003) from NIFS
Aug. 2003

NIFS-781 Ya. I. Kolesnichenko, K. Yamazaki, S. Yamamoto, V.V. Lutsenko, N. Nakajima, Y. Narushima, K. Toi, Yu. V. Yakovenko
Interplay of Energetic Ions and Alfvén Modes in Helical Plasmas
Aug. 2003

NIFS-782 S.-I. Itoh, K. Itoh and M. Yagi
Turbulence Trigger for Neoclassical Tearing Modes in Tokamaks
Sep. 2003

NIFS-783 F. Spineanu, M. Vlad, K. Itoh, H. Sanuki and S.-I. Itoh
Pole Dynamics for the Flierl-Petviashvili Equation and Zonal Flow
Sep. 2003

NIFS-784 R. Smirnov, Y. Tomita, T. Takizuka, A. Takayama, Yu. Chutov
Particle Simulation Study of Dust Particle Dynamics in Sheaths
Oct. 2003

NIFS-785 T.-H. Watanabe and H. Sugama
Kinetic Simulation of Steady States of Ion Temperature Gradient Driven Turbulence with Weak Collisionality
Nov. 2003

NIFS-786 K. Itoh, K. Hallatschek, S. Toda, H. Sanuki and S.-I. Itoh
Coherent Structure of Zonal Flow and Nonlinear Saturation
Dec. 2003

NIFS-787 S.I. Itoh, K. Itoh, M. Yagi and S. Toda
Statistical Theory for Transition and Long-time Sustainment of Improved Confinement State
Dec. 2003

NIFS-788 A. Yoshizawa, S.-I. Itoh, K. Itoh and N. Yokoi
Dynamos and MHD Theory of Turbulence Suppression
Dec. 2003

NIFS-789 V.D. Pustovitov
Pressure-induced Shift of the Plasma in a Helical System with Ideally Conducting Wall
Jan. 2004

NIFS-790 S. Koikari
Rooted Tree Analysis of Runge-Kutta Methods with Exact Treatment of Linear Terms
Jan. 2004

NIFS-791 T. Takahashi, K. Inoue, N. Iwasawa, T. Ishizuka and Y. Kondoh
Losses of Neutral Beam Injected Fast Ions Due to Adiabaticity Breaking Processes in a Field-Reversed Configuration
Feb. 2004